International Journal of Minerals, Metallurgy and Materials
Volume 21, Number 9, September 2014, Page 913
DOI: 10.1007/s12613-014-0989-3

Effects of environmental factors on corrosion behaviors of metal-fiber porous components in a simulated direct methanol fuel cell environment

Wei Yuan, Bo Zhou, Yong Tang, Zhao-chun Zhang, and Jun Deng

Key Laboratory of Surface Functional Structure Manufacturing of Guangdong Higher Education Institutes, School of Mechanical and Automotive Engineering, South China University of Technology, Guangzhou 510640, China

(Received: 13 December 2013; revised: 11 March 2014; accepted: 20 March 2014)

Abstract: To enable the use of metallic components in direct methanol fuel cells (DMFCs), issues related to corrosion resistance must be considered because of an acid environment induced by the solid electrolyte. In this study, we report the electrochemical behaviors of metal-fiber-based porous sintered components in a simulated corrosive environment of DMFCs. Three materials were evaluated: pure copper, AISI304, and AISI316L. The environmental factors and related mechanisms affecting the corrosion behaviors were analyzed. The results demonstrated that AISI316L exhibits the best performance. A higher SO_4^{2-} concentration increases the risk of material corrosion, whereas an increase in methanol concentration inhibits corrosion. The morphological features of the corroded samples were also characterized in this study.

Keywords: corrosion; metal fibers; porous; sintering; direct methanol fuel cells; environmental factors

1. Introduction

The emergence of fuel-cell technology illuminates the opportunity for replacing traditional combustion engines and secondary batteries by virtue of fuel cells' advantages such as higher energy efficiency and lower pollutant emissions [1–2]. As a promising candidate, the direct methanol fuel cell (DMFC) has attracted considerable attention and is structurally similar to the popular hydrogen-based proton exchange membrane (PEM) fuel cell. A DMFC uses methanol directly as the fuel source without a reforming process, which allows a more compact system structure and correspondingly higher energy density; DMFCs thereby exhibit great potential for use in portable applications [3–4].

As a core component of the DMFC, the bipolar plate with patterned flow fields not only helps distribute the reactants and products but also serves as a current collector. In most of the early studies on DMFCs, non-porous graphite was used in the fabrication of such components because of its good electrical conductivity and high chemical stability in the harsh environment of a PEM-based fuel cell [5–7]. However, the graphite plate is brittle, and therefore lacks mechanical resistance to external vibration; this brittleness also results in higher production costs related to the creation of flow fields. With this background, numerous researchers have attempted to use metal as an alternative to graphite [8]. In contrast to graphite, metals are more machinable and exhibit a greater mechanical strength. Thus, a wide variety of shaping methods, such as cutting, stamping, etching, and even rapid prototyping, can be used to fabricate metallic components that can be made very thin to reduce both the amount of material used and the system volume. Despite these alluring properties, researchers who investigate the use of metal components in DMFCs must consider the aggressive environment in such fuel cells, which are based on perfluorosulfonic acid membranes such as the Nafion® series manufactured by Dupont™. If the metal corrodes, the released elements inevitably poison the catalysts and hurt the membrane. Such effects must be avoided because they will substantially reduce the long-term performance and durability of fuel cells. The open literature contains extensive reports on the corrosion phenomena and anti-corrosion technology with regard to various metals and alloys [9–16].

Corresponding author: Wei Yuan E-mail: mewyuan@scut.edu.cn

However, most previous reports have focused on the environment in hydrogen-fed PEM fuel cells. Detailed information concerning DMFCs in this field is scarce, although a few groups have used solid and porous metallic materials to fabricate DMFC components including the flow distributor, diffusion medium, and current collector [17–19].

To this end, we recently reported the corrosion behaviors of several potential metallic materials in both simulated and actual DMFC environments [20]. We intended to create thin fibers from these materials for fabricating a porous sintered flow distributor, which serves as an anodic mass-transfer-controlling medium in a passive DMFC to optimize the management of multiphase flow. However, we reported only preliminary results related to the electrochemical and morphological characteristics of the candidate materials under corrosive conditions. As an extension of our previous study, we presented additional information about the effects of environmental factors on the candidate materials in this paper.

2. Experimental

In this study, we selected three fiber-based metallic materials for corrosion evaluation (Table 1). The tested samples are shown in Fig. 1. The fibers constructed of pure copper and AISI304 were produced by low-speed cutting with a super-hard multitooth cutter on a horizontal lathe, as shown in Fig. 2. A row of triangle microteeth were machined on the cutting face of this tool so as to produce a string of continuous long fibers with diameters of 50–100 μm at one time. The fibers were cleaned, segmented, loaded into a mold assembly, and then sintered in a resistance furnace. By adjusting the cutter geometry, cutting parameters, and sintering conditions, we could control the structure and morphology of the fibers and sintered felts. Furthermore, we could adaptively optimize their mechanical properties and functional characteristics. In this experiment, the porosities of all the samples were 80%. More information about the processing parameters is available elsewhere [21].

Table 1. Three types of porous metallic materials investigated in this study

Sample No.	Material	Fiber production method	Major element content / wt%	Sintering conditions
1#	Copper	Multi-tooth cutting	Cu: ≥ 99.9	0.3 MPa (hydrogen atmosphere); 5ºC·min^{-1}; 900ºC for 1 h; furnace cooling
2#	AISI304	Multi-tooth cutting	Cr: 18–20; Ni: 8–10; Mn: ≤ 2; Si: ≤ 1	40 Pa (vacuum); 5ºC·min^{-1}; 1200ºC for 1 h; furnace cooling
3#	AISI316L	Bundle drawing	Cr: 16–18; Ni: 10–14; Mo: 2–3; Mn: ≤ 2; Si: ≤ 1	Purchased

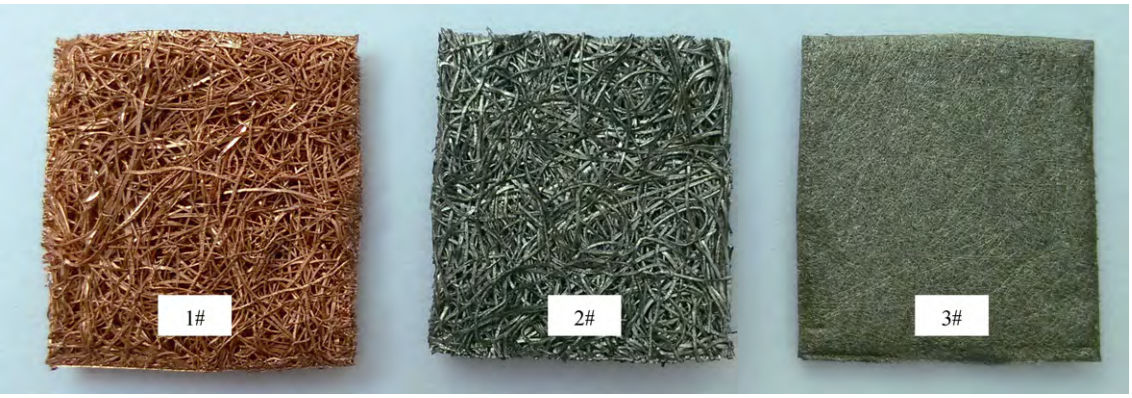

Fig. 1. Photos of three types of porous metallic samples.

The effective size of the tested samples was 15 mm × 12 mm × 2.5 mm. Before being tested, the samples were cleaned ultrasonically with acetone and then with deionized water and were finally dried in air. A simulated solution composed of specified amounts of sulfuric acid (H_2SO_4), hydrofluoric acid (HF), and methanol (CH_3OH) was prepared. To evaluate the effects of environmental factors, we prescribed different solution compositions, as listed in Table 2. The cathode solution was bubbled to simulate the air-breathing mode of a practical DMFC.

The electrochemical experiments were conducted using a three-electrode system on an electrochemical workstation (AUTOLAB PGSTAT302). The ambient temperature was maintained at 25°C. Platinum foil (Pt ≥ 99.95wt%, 20 mm × 15 mm × 0.2 mm) was used to prepare the auxiliary electrode, whereas a saturated calomel electrode (SCE) was used as the reference electrode. Unless otherwise specified, all electrode potentials were referenced to the SCE. For po-

tentiodynamic polarization measurements, the scan rate was maintained at 1 $mV \cdot s^{-1}$ ranging from −0.5 to 1.5 V. Before each run, the sample was first stabilized under open-circuit conditions for 30 min. The surface morphology of each sample was characterized by micrographic methods.

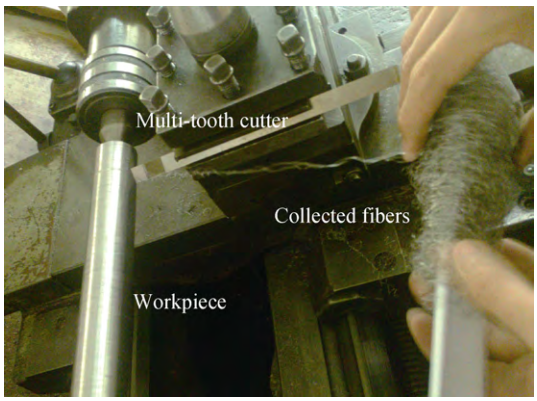

Fig. 2. Multi-tooth cutting for metal fiber production.

Table 2. Compositions of simulated environments

Electrode	Simulated DMFC environment	SO_4^{2-} / ($mol \cdot L^{-1}$)	$CH_3OH_4^{2-}$ / ($mol \cdot L^{-1}$)	F^- / wt%
Anode	High SO_4^{2-}	2.0	2.0	2×10^{-4}
	Low SO_4^{2-}	0.5	2.0	2×10^{-4}
	High CH_3OH	1.0	8.0	2×10^{-4}
	Low CH_3OH	1.0	0.5	2×10^{-4}
Cathode	High SO_4^{2-}	2.0	0.01 (Methanol crossover)	2×10^{-4}
	Low SO_4^{2-}	0.5	0.01 (Methanol crossover)	2×10^{-4}

3. Results and discussion

3.1. Electrochemical corrosion behavior

Figs. 3–5 compare the polarization behaviors of the three samples in simulated anode and cathode environments of a DMFC when solutions with different compositions were used. With respect to sample 1#, no activation-to-passivation transfer was apparent in its polarization curves. The emergence of multiple corrosion potentials in the negative region in Figs. 3 and 4 suggests that the system was still in chaos because the pure copper was easily oxidized. A relatively stable stage was observed, indicating that a balance status was formed in this section. After the potential was increased to approximately −0.05 V, the current rapidly increased to a very high value with a magnitude of 10^{-1} A. We further noted that the current continued increasing at the point where the anode working potential was applied (0.2 V), which suggests that the material underwent continuous dissolution in this case. The two polarization curves of sample 1# are almost coincident, showing obvious insensitivity to the SO_4^{2-} concentration. This behavior implies that the effect of this acid ion can be neglected. In contrast, an increase in methanol concentration tended to slightly shift the curve rightward, which indicates that the use of a higher methanol

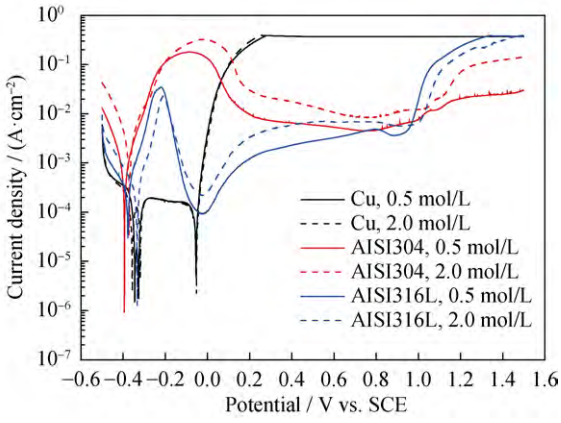

Fig. 3. Effects of SO_4^{2-} concentration on polarization behaviors in the simulated DMFC anode environment.

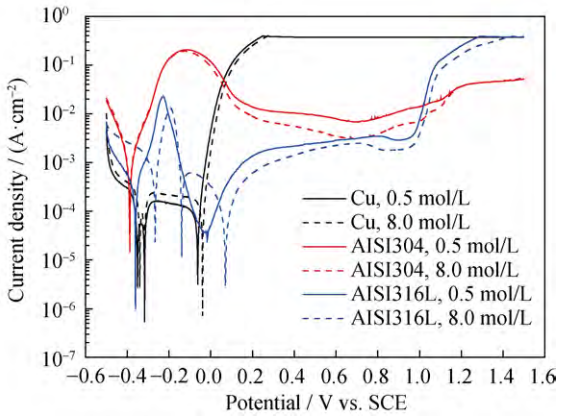

Fig. 4. Effects of CH_3OH concentration on polarization behaviors in the simulated DMFC anode environment.

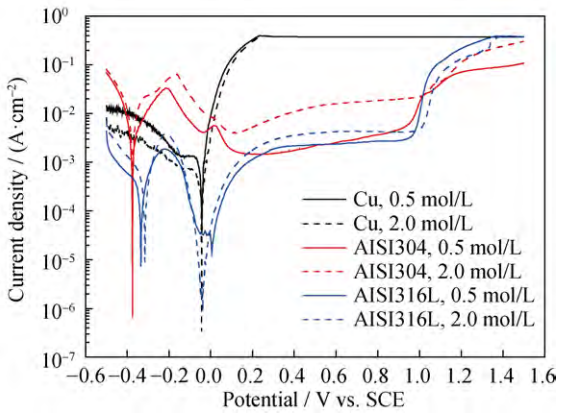

Fig. 5. Effects of SO_4^{2-} concentration on polarization behaviors in the simulated DMFC cathode environment.

concentration possibly enhances the corrosion resistance via the formation of a local protective area near the sample surface. In the case of the cathode environment (see Fig. 5), the point of the applied cathode working potential (0.7 V) is located in the high-current region, indicating that pure copper cannot withstand corrosion in this environment.

Figs. 3–5 also illustrate the corrosion behaviors of samples 2# and 3#. The anode and cathode polarization curves indicate an activation-to-passivation transfer process. After this transience, the curves return to a relatively stable stage, reflecting the formation of a stable passive film on the material surface. The current at both the applied anode and cathode potentials resided in the stable passivation regions, suggesting that both AISI304 and AISI316L exhibit good corrosion resistance under the simulated conditions. We further noted that the SO_4^{2-} concentration of 2.0 mol·L^{-1} promoted a higher corrosion current than the SO_4^{2-} concentration of 0.5 mol·L^{-1}. This result agrees well with the rationale of electrochemical corrosion, which indicates that a higher SO_4^{2-} concentration leads to a higher corrosion rate. When a higher concentration of SO_4^{2-} is used, more acid ions contact the passive film. In this case, the electrical conductivity between the tested sample and the solution must be enhanced so as to lower the corrosion resistance of the material. Fig. 4 shows that the current corresponding to a methanol concentration of 8.0 mol·L^{-1} is lower than that corresponding to a concentration of 0.5 mol·L^{-1} in the passivation region. This lower current can be attributed to the decrease in electrical conductivity of the working solution. Another possible reason for this phenomenon is the fact that the addition of CH_3OH facilitates the formation of a shield layer that protects the passive film from extreme corrosion. Notably, the polarization curve of sample 3# exhibited two minimum values of current density in the negative-voltage region when 8.0 mol·L^{-1} methanol was used. This phenomenon can be ascribed to the use of a higher methanol concentration and also to the corrosion resistance of AISI316L. These two factors combine to facilitate the emergence of an alternant process of formation and dissolution of the passive film with the increase in load potential.

Although the polarization curve for sample 3# exhibits a profile similar to that of sample 2#, it indicates a much lower magnitude of corrosion current compared to that of sample 2#. Meanwhile, the corrosion potential of sample 3# becomes more positive than that of sample 2#. These results confirm that AISI316L performs better than AISI304 in the simulated DMFC environment. This better performance of AISI316L is attributed to the inclusion of molybdenum and to its higher nickel content, which enhances its corrosion resistance. Another noteworthy phenomenon is that the current of sample 3# exhibits a sharp decrease before reaching the stable stage. This profile reveals that the material continues to resist corrosion under the increasing potential until forms a stable passive film. The curves related to sample 3# again confirm that a higher SO_4^{2-} concentration promotes corrosion, whereas a higher methanol concentration reduces the degree of corrosion. Thus, we inferred that the use of a concentrated fuel is favorable to resist corrosion of fuel cell components. The merit of this advantage lies in the high-concentration operation, which will significantly enhance the energy density and prolong the operating time of a DMFC.

3.2. Morphological description

Figs. 6–8 describe the morphological features of the three samples before and after corrosion tests. As evident from results in Fig. 6, the color of the copper fiber changed from bright yellow to dark brown with burr-like structures formed and distributed on its surface. Such obvious changes in both color and surface structure can be ascribed to the oxidization of copper in the simulated DMFC environment [20]. In view of the AISI304 fibers, a few distinct yellow spots appeared on its surface after corrosion, as shown in Fig. 7. Austenitic stainless steel is known to exhibit a higher corrosion

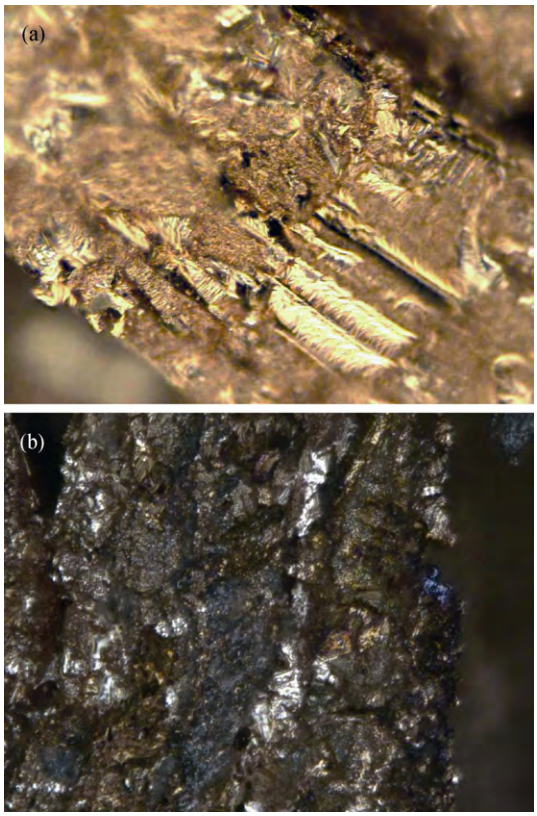

Fig. 6. Morphological characterization of sample 1# before (a) and after (b) corrosion.

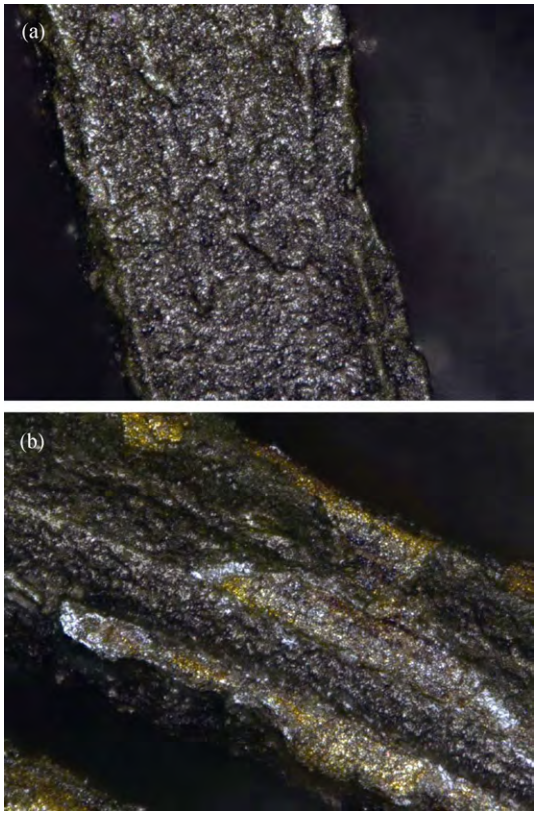

Fig. 7. Morphological characterization of sample 2# before (a) and after (b) corrosion.

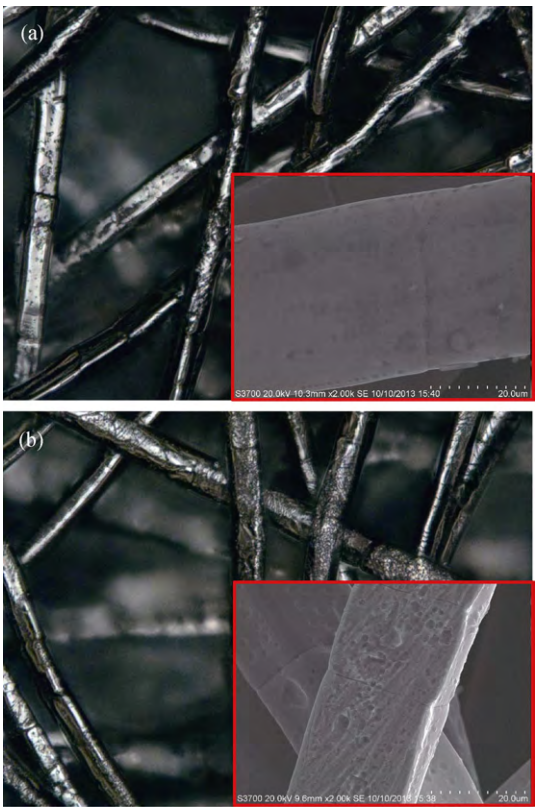

Fig. 8. Morphological characterization of sample 3# before (a) and after (b) corrosion.

resistance when a dense chromium-rich oxide film, which prevents continuous penetration of the corrosive medium, is formed on its surface. When tested in the acid environment, the protective film might be oxidized by the oxidizing solution to produce a yellow-colored chromate solution. Fig. 8 shows the appearance of the AISI316L fibers produced by the bundle-drawing technique. Compared with the fibers prepared by cutting, such fibers have a relatively smoother surface. After undergoing corrosion, the fiber surface becomes very coarse because of the formation of numerous micropores/cavities on its surface, which can be verified by the magnified view of fibers (see bottom-right SEM images in Fig. 8).

4. Conclusions

(1) Among the three tested samples, pure copper performed the worst in the simulated DMFC environment. The stainless steel AISI304 and AISI316L samples both exhibited good corrosion resistance because of the formation of a passive film at the applied potentials. Further comparison revealed that AISI316L performed better than AISI304.

(2) Copper exhibited a less sensitivity to the change in SO_4^{2-} concentration, which strongly affected stainless steel. A higher concentration of SO_4^{2-} tended to promote corrosion. These results suggest that the methanol concentration used in DMFCs should be increased to mitigate corrosion, consistent with the aim of realizing high-concentration operation of a practical DMFC to enhance its energy density and operating time.

(3) Microscopic characterization revealed that non-visualized destroyed traces were present on the surface of AISI316L. From the perspective of long-term applications, the exploration of effective anticorrosion methods is important to protect AISI316L from corrosion in a DMFC environment.

Acknowledgements

This work was financially supported by the Natural Science Foundation of Guangdong Province, China (No. S2013040016899), the Fundamental Research Funds for Central Universities of China (No. 2013ZM0003), the National Natural Science Foundation of China (No. 51275180), and the Open Fund of Shanghai Key Laboratory of Digital Manufacture for Thin-walled Structures (No. 2013001).

References

[1] G. Hoogers, A. Bauen, E. Chen, D. Hart, M. Hinsberger, M.

Hogarth, R. Stone, and D. Thompsett, *Fuel Cell Technology Handbook*, CRC Press, Boca Raton, 2003, p. 1.

[2] C.K. Dyer, Fuel cells for portable applications, *J. Power Sources*, 106(2002), No. 1-2, p. 31.

[3] W.M. Qian, D.P. Wilkinson, J. Shen, H.J. Wang, and J.J. Zhang, Architecture for portable direct liquid fuel cells, *J. Power Sources*, 154(2006), No. 1, p. 202.

[4] A.S. Aricò, S. Srinivasan, and V. Antonucci, DMFCs: from fundamental aspects to technology development, *Fuel Cells*, 1(2001), No. 2, p. 133.

[5] J.S. Cooper, Design analysis of PEMFC bipolar plates considering stack manufacturing and environment impact, *J. Power Sources*, 129(2004), No. 2, p. 152.

[6] W. Schmittinger and A. Vahidi, A review of the main parameters influencing long-term performance and durability of PEM fuel cells, *J. Power Sources*, 180(2008), No. 1, p. 1.

[7] J.F. Wu, X.Z. Yuan, J.J. Martin, H.J. Wang, J.J. Zhang, J. Shen, S.H. Wu, and W. Merida, A review of PEM fuel cell durability: degradation mechanisms and mitigation strategies, *J. Power Sources*, 184(2008), No. 1, p. 104.

[8] H. Tawfik, Y. Hung, and D. Mahajan, Metal bipolar plates for PEM fuel cell: a review, *J. Power Sources*, 163(2007), No. 2, p. 755.

[9] R.A. Antunes, M.C.L. Oliveira, G. Ett, and V. Ett, Corrosion of metal bipolar plates for PEM fuel cells: a review, *Int. J. Hydrogen Energy*, 35(2010), No. 8, p. 3632.

[10] H.L. Wang, M.A. Sweikart, and J.A. Turner, Stainless steel as bipolar plate material for polymer electrolyte membrane fuel cells, *J. Power Sources*, 115(2003), No. 2, p. 243.

[11] P.Y. Yi, L.F. Peng, T. Zhou, J.Q. Huang, and X.M. Lai, Composition optimization of multilayered chromium-nitride-carbon film on 316L stainless steel as bipolar plates for proton exchange membrane fuel cells, *J. Power Sources*, 236(2013), p. 47.

[12] P.Y. Yi, L.F. Peng, T. Zhou, H. Wu, and X.M. Lai, Development and characterization of multilayered Cr–C/a–C:Cr film on 316L stainless steel as bipolar plates for proton exchange membrane fuel cells, *J. Power Sources*, 230(2013), p. 25.

[13] C.H. Liang, C.H. Cao, and N.B. Huang, Electrochemical behavior of 304 stainless steel with electrodeposited niobium as PEMFC bipolar plates, *Int. J. Miner. Metall. Mater.*, 19(2012), No. 4, p. 328.

[14] Y. Yang, L.J. Guo, and H.T. Liu, Factors affecting corrosion behavior of SS316L as bipolar plate material in PEMFC cathode environments, *Int. J. Hydrogen Energy*, 37(2012), No. 18, p. 13822.

[15] R. Włodarczyk and A. Wronska, Effect of pH on corrosion of sintered stainless steels used for bipolar plates in polymer exchange membrane fuel cells, *Arch. Metall. Mater.*, 58(2013), No. 1, p. 89.

[16] S. Lædre, O.E. Kongstein, A. Oedegaard, F. Seland, and H. Karoliussen, The effect of pH and halides on the corrosion process of stainless steel bipolar plates for proton exchange membrane fuel cells, *Int. J. Hydrogen Energy*, 37(2012), No. 23, p. 18537.

[17] R. Chen and T.S. Zhao, Porous current collectors for passive direct methanol fuel cells, *Electrochim. Acta*, 52(2007), No. 13, p. 4317.

[18] T. Shudo and K. Suzuki, Performance improvement in direct methanol fuel cells using a highly porous corrosion-resisting stainless steel flow field, *Int. J. Hydrogen Energy*, 33(2008), No. 11, p. 2850.

[19] J.G. Liu, G.Q. Sun, F.L. Zhao, G.X. Wang, G. Zhao, L.K. Chen, B.L. Yi, and Q. Xin, Study of sintered stainless steel fiber felt as gas diffusion backing in air-breathing DMFC, *J. Power Sources*, 133(2004), No. 2, p. 175.

[20] W. Yuan, Y. Tang, X. Yang, L. Bu, and Z. Wan, Corrosion behavior of porous metal fiber-sintered felt in both simulated and practical environments of a direct methanol fuel cell, *Corrosion*, 69(2013), No. 1, p. 25.

[21] W. Yuan, Y. Tang, X.J. Yang, and Z.P. Wan, Toward using porous metal-fiber sintered plate as anodic methanol barrier in a passive direct methanol fuel cell, *Int. J. Hydrogen Energy*, 37(2012), No. 18, p. 13510.